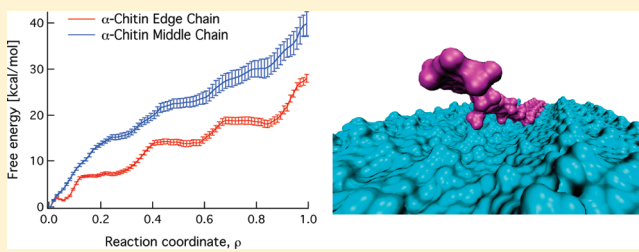


Examination of the α -Chitin Structure and Decrystallization Thermodynamics at the Nanoscale

Gregg T. Beckham^{*,†,‡,§} and Michael F. Crowley[¶][†]National Bioenergy Center, National Renewable Energy Laboratory, Golden Colorado 80202, United States[‡]Department of Chemical Engineering, Colorado School of Mines, Golden Colorado 80202, United States[§]Renewable and Sustainable Energy Institute, Boulder Colorado 80302, United States[¶]Biosciences Center, National Renewable Energy Laboratory, Golden Colorado 80202, United States**S Supporting Information**

ABSTRACT: Chitin is the primary structural material of insect and crustacean exoskeletons and fungal and algal cell walls, and as such it is one of the most abundant biological materials on Earth. Chitin forms linear polymers of β 1,4-linked-N-acetyl-D-glucosamine (GlcNAc), and in Nature, enzyme cocktails deconstruct chitin to GlcNAc. The mechanism of chitin deconstruction, like that of cellulose deconstruction, has been under investigation due to its importance in the global carbon cycle and in production of renewable and sustainable products from biological matter. To further understand the nanoscale properties of chitin, here we simulate crystals of α -chitin, which is the most prevalent form in Nature. We find excellent agreement with the recently reported crystal structure and we report the salient features of the simulations related to crystalline stability. We also compute the thermodynamic work required to peel individual chains from α -chitin surfaces, which a chitinase enzyme must conduct to deconstruct chitin. Compared with previous simulations of native plant cellulose I β , α -chitin exhibits higher decrystallization work for chains in the middle of surfaces and similar work for chains on the edges of crystals. Unlike cellulose, the free energy profile is dominated by a single bifurcated hydrogen bond between chains formed by the GlcNAc side chains and the O6 atoms on the primary alcohol group. This study highlights the molecular features of chitin that make it such a tough, recalcitrant material, and provides a key thermodynamic parameter in our quantitative understanding of how enzymes contribute to the turnover of carbohydrates in the biosphere.



INTRODUCTION

Chitin is the linear polymer of β -1,4-N-acetyl-D-glucosamine (GlcNAc), and after cellulose it is the second most abundant biological material on Earth. Chitin forms a vital component of the exoskeletal materials of crustaceans, insects, and mollusks and the cell wall material in fungi and algae.^{1,2} Additionally, chitin and its deacetylated derivative chitosan are useful functional materials that have many industrial, medical, agricultural, food, and environmental applications.^{3–9} The conformational monomer of chitin is the GlcNAc dimer, or chitobiose. Polymers of chitin are synthesized as crystalline fibrils, similar to cellulose, of hundreds to thousands of monomer units long. In Nature, chitin exists in two crystalline forms including the most naturally prevalent form, α -chitin, which is synthesized in an antiparallel fashion, similar to cellulose II.^{10–12} The other naturally occurring form is β -chitin, which occurs only rarely and has been observed in a hydrate form.^{13,14} The molecular structure of α -chitin was proposed originally by Minke and Blackwell¹² and was recently re-examined by Sikorski et al. using synchrotron X-ray diffraction data from highly crystalline samples obtained from crab.¹¹ The unit cell of α -chitin consists of two chitobiose molecules forming two separate chains in the crystal. The α -chitin structure also

exhibits a distinct, three-dimensional hydrogen bonding pattern and the hydrophobic faces of the carbohydrate rings stack on top of one another. These features are likely central to the ability of chitin to act as an insoluble, recalcitrant material for structure and defense.¹⁵

The degradation of chitin in the biosphere is accomplished by synergistic enzyme cocktails and is an essential component of the global carbon cycle. Processive chitinase enzymes in particular provide a significant amount of hydrolytic potential, similar to processive enzymes for degrading cellulose.^{15–21} Processive chitinases are able to acquire a chitin chain from a polymer crystal and hydrolyze the glycosidic linkages sequentially. Because the structure of α -chitin exhibits both significant hydrogen bonding and hydrophobic interactions, processive enzymes must overcome a free energy barrier to decrystallize an individual chitin chain from the surface of a crystalline fibril, which is related directly to the ligand binding free energy in an enzyme tunnel or cleft.^{22–26} This decrystallization work is likely dependent on the

Received: January 27, 2011**Revised:** March 17, 2011**Published:** March 31, 2011

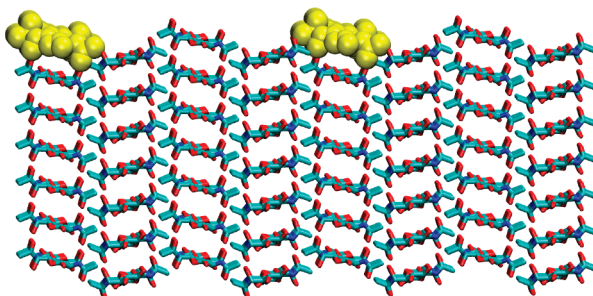


Figure 1. Two independent decrystallization scenarios for α -chitin examined in this study. We decrystallized chains on the surface from a corner and a middle chain as highlighted in yellow. The bottom three layers were removed after 10 ns of equilibration at 300 K.

location of the chitin chain on the surface, as it was shown to be in cellulose.²⁷ Moreover, the free energy change to decrystallize a chitin chain, thread it into an enzyme, hydrolyze it to chitobiose, and expel the product must be thermodynamically downhill as chitinases act extra-cellularly and do not utilize ATP.

Computational approaches offer an effective means to probe the structure and decrystallization thermodynamics of chitin at the nanoscale.^{27–30} Here we present the first molecular dynamics (MD) simulations of α -chitin to our knowledge starting from the recently refined crystal structure.¹¹ We find excellent agreement between the simulated crystal and the experimental lattice parameters. Additionally, we use free energy methods to calculate the amount of work required to decrystallize chitin chains from the surface of the chitin fibrils. This thermodynamic quantity is the amount of work that a processive chitinase enzyme must compensate for by threading the chitin chain into the enzyme tunnel or cleft.

METHODS

We used the CHARMM program for all of our simulations.³¹ The starting coordinates were built from the recently refined crystal structure.¹¹

Equilibration Simulations. The initial crystal was 20 GlcNAc units long with 8 chains in a given layer and 7 chain layers deep for a crystal of 1120 GlcNAc units as shown in Figure 1. The crystal was solvated with water for a system of approximately 76 000 atoms, minimized for 1000 steps with steepest descent minimization, and heated from 50 to 300 K in increments of 50 K for 2000 MD steps per temperature window with a 1 fs time step. The crystal was then equilibrated at 300 K in the *NVT* ensemble for 50 ps, and then in the *NPT* ensemble for 500 ps for density equilibration. The time step for all MD simulations was 2 fs after heating. The Nosé–Hoover thermostat was used for temperature control.^{32,33} The recently developed C35 force field^{34,35} was used to describe chitin and the TIP3P model was used to describe water.³⁶ The SHAKE algorithm was used to fix the distances to all hydrogen atoms.³⁷ We used a 12 Å cutoff for nonbonded interactions and the Particle Mesh Ewald method was used to describe the electrostatics with a sixth order spline.³⁸

An equilibration production run for this large crystal was conducted for 10 ns. This simulation time was determined to be adequate based on the stable root-mean-square deviation of the crystal as a function of time as shown in Figure S1 in the Supporting Information. The last 8 ns of the production run were used to examine the hydrogen bonding structure and the

lattice parameters for comparison to the experimentally determined crystal structure, similar to previous work on cellulose from multiple groups.^{30,39–42} Lattice parameters were calculated from chains in the interior of the crystal as shown in Figure S2 in the Supporting Information. As in our previous work, we defined a hydrogen bond below a donor–acceptor distance threshold of 3.4 Å and 60° from linear.²⁷ We examined the number, types, and occupancies of hydrogen bonds on the surface of the crystal, the interior, and the chains of interest for the decrystallization simulations. In addition, we calculated the root-mean-square fluctuations of the heavy ring atoms of the polymers for the last 8 ns of the equilibration run to determine the relative stabilities of the chains as a function of morphology.

Decrystallization Simulations. From the equilibrated structure, the bottom three layers of the crystal were removed to produce a crystal of 640 GlcNAc molecules (Figure 1 shows the full 1120 molecule crystal). The new bottom layer was then harmonically restrained with a force constant of 2.0 kcal/mol/Å² on the ring atoms of each monomer unit. In addition, we added sufficient water to the simulation cell to avoid the chain of interest being decrystallized from interacting with its periodic image. The total system size for the free energy calculations was approximately 72 000 atoms. From this structure, we ran two independent free energy simulations to examine the dependence of the chain location on the work required to peel the chain off the surface, as an enzyme would have to do to deconstruct chitin. Figure 1 shows the two chains of interest in yellow that were peeled off the surface of the chitin crystal. The surface in Figure 1 was chosen because it is likely the hydrophobic face in crystalline chitin that carbohydrate-binding modules in chitinases will bind to, based on related findings for cellulose.^{43–45}

The free energy simulations were conducted with MD umbrella sampling.^{46,47} The reaction coordinate we used describes the fraction of native contacts of the chain of interest to be peeled from the surface to the remainder of the crystal as described by Sheinerman and Brooks for protein folding.⁴⁸ Specifically, we chose eight GlcNAc monomers starting at the reducing end in the chain of interest in the primary set and all other monomers in the crystal except those in the chain of interest in the secondary set to define native contacts. The distance cutoff for the native contacts corresponds to the nonbond cutoff distance of 12 Å to ensure that the decrystallized chains do not interact with the crystal. Reference 27 provides a more detailed discussion of this reaction coordinate applied to polymer chain decrystallization. Windows were run for 10 ns each from a reaction coordinate value of $\rho = 0$ where all native contacts are formed to $\rho = 1$ where all native contacts were broken. The window center interval was 0.025 along ρ , which corresponds to 41 windows total and 0.41 ms of simulation time per decrystallization scenario to ensure convergence. The chain of interest was decrystallized by approximately 5 nm as was done previously for cellulose chains in four cellulose polymorphs.²⁷ The umbrella sampling simulations were analyzed with the weighted histogram analysis [WHAM] method⁴⁹ and error analysis on the potential of mean force was conducted with bootstrapping.

RESULTS AND DISCUSSION

We describe the results for simulations of the crystal structure and the free energy results from the decrystallization umbrella sampling runs in turn.

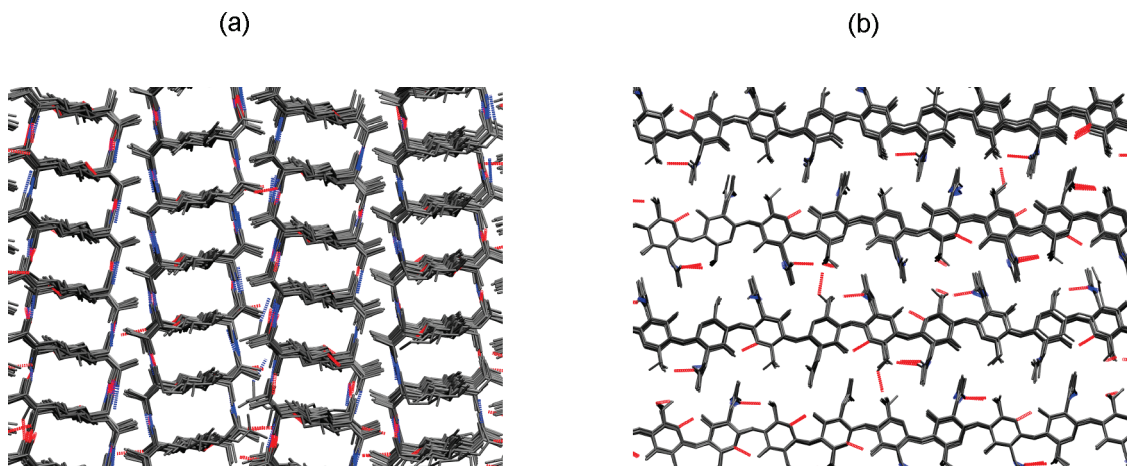


Figure 2. Snapshot of the hydrogen-bonding patterns in α -chitin after 10 ns of equilibration. Hydrogen bonds in blue are to nitrogen and red hydrogen bonds are between oxygens. (a) View down the c -axis. (b) View down the a -axis.

Table 1. The Lattice Parameters and Angles from Experiment and Simulation^a

parameter	simulation	experimental ¹¹
a [Å]	4.69 (0.16)	4.749 (0.07)
b [Å]	19.02 (0.19)	18.89 (0.14)
c [Å]	10.32 (0.09)	10.33 (0.10)
α	90.0° (1.1°)	90°
β	90.0° (2.5°)	90°
γ	90.0° (2.3°)	90°

^a For the simulation data, we report 1 standard deviation in parentheses.

Table 2. Hydrogen Bonding Behavior of Surface Chains from Figure 1 in the α -Chitin Crystal^a

edge chain	self	20.1 (2.8)
	intralayer	2.4 (1.3)
	interlayer	32.8 (2.0)
middle surface chain	self	22.7 (2.1)
	intralayer (even)	1.1 (0.8)
	intralayer (odd)	3.9 (1.5)
	interlayer	40.7 (2.1)

^a In parentheses, we report 1 standard deviation from the mean.

Crystal Structure. The results for the crystal lattice parameters and lattice angles are shown in Table 1 with the experimental values.¹¹ We report one standard deviation on the lattice constants from the mean. As shown, the lattice constants are in excellent agreement with the experimental values, which is typically a difficult problem for classical force fields to describe organic crystals.^{50–52} Unlike in some cellulose simulations of finite crystals,⁴⁰ the chitin fibril does not adopt a twisted conformation.

We also examined the hydrogen bonding patterns of the chitin crystal as a function of location in the crystal as shown in Table 2 and Figures 2 and 3. The hydrogen-bonding pattern in α -chitin adopts a stable network of hydrogen bonds between layers of adjacent chitin chains mediated by the GlcNAc side chain interactions with adjacent GlcNAc side chains and the O6 side chains. Figure 2 shows that the hydrogen bonds to nitrogen (in blue) are primarily in a vertical direction (i.e., along the a -axis)

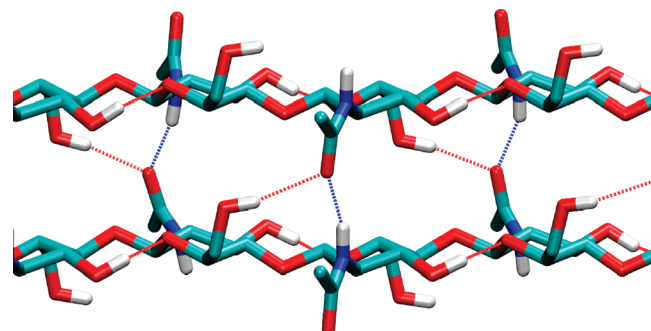


Figure 3. Bifurcated hydrogen bonds are formed between the GlcNAc side chain and the O6 side chain of every 2 residues in a layer to the GlcNAc side chain in the layer above. These hydrogen bonds are the interlayer hydrogen bonds in Table 2. The hydrogen bonds internal to a chain between O5 and O3/HO3 are self-hydrogen bonds in Table 2.

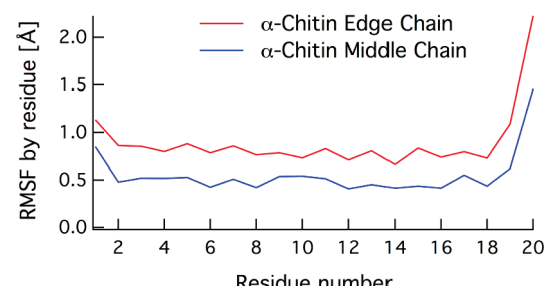


Figure 4. RMSF as a function of chain and residue number for the two surface chains of interest.

and hydrogen bonds between oxygens are along the c -axis (in red). The primary, bifurcated hydrogen bond (which exhibits high occupancy) in α -chitin is shown in Figure 3, which is formed between adjacent GlcNAc side chains between chain layers. The primary alcohol O6 and HO6 atoms also participate in this bifurcated hydrogen bond along the chains. Also from Figures 2 and 3, there are hydrogen bonds internal to a chain (self-hydrogen bonds in Table 2). These hydrogen bonds are between the O5 atoms on the ring and the O3 atoms on the neighboring residue along the chain.

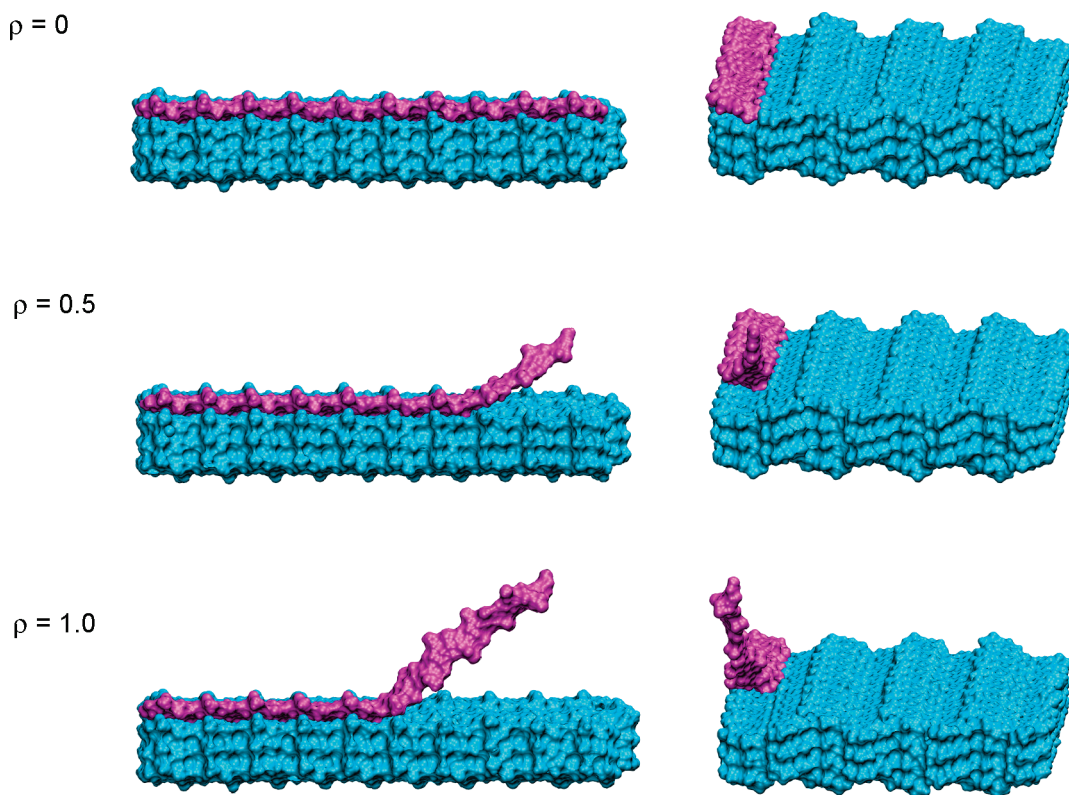


Figure 5. α -chitin decrystallization as a function of the reaction coordinate at $\rho = 0.0, 0.5$, and 1.0 from two views from the edge chain decrystallization trajectories. The chain of interest is highlighted in magenta.

Table 2 shows the hydrogen bonding patterns for the two chains of interest on the crystal surface. Table S1 in the Supporting Information provides the hydrogen bonding information for chains interior to the crystal.

Also, we examined the RMSF of the chains in the crystal to examine the relative lattice stability as a function of morphology. Here we report the average RMSF for the two chains of interest on the surface (the chains highlighted in Figure 1) in Figure 4 and for representative interior, surface, and edge chains and in the Supporting Information (Figure S2) as a function of the chain and residue number. As shown, the ends of the surface chains exhibit significant fluctuations. The reducing ends of the polymer chains (residue 20 in both cases) exhibit significantly higher fluctuations than the nonreducing ends. As shown in Figure S2, however, the interior chains do not exhibit significant fluctuation along the length of the entire chain, as expected.

Free Energy of Decrystallization. Figure 5 shows snapshots for the edge chain at several values of the reaction coordinate. Figure S3 in the Supporting Information shows similar snapshots for the middle chain decrystallization trajectories. As intended, the chain exhibits significant conformational flexibility in solution. The free energy calculated here is thus the difference between the free energy of the flexible chain in solution still bonded to the chain in the crystal along with new surfaces exposed from the free energy of the entire chain in the crystal. This quantity is the work that a chitinase enzyme must perform to decrystallize and bind a single polymer chain of chitin into an active site tunnel. Thus, the decrystallization work is directly comparable to the chitinase ligand binding free energy. Modifying the ligand binding free energy, for example, by mutating

aromatic residues in chitinase tunnels to smaller, nonpolar residues, will thus hinder the ability of a chitinase to form a catalytically active complex.^{18,19} Moreover, the work values calculated here quantify the molecular level, intrinsic thermodynamic stability of α -chitin chains as a function of morphology on the crystal surface.

The free energy of decrystallization for both scenarios is shown in Figure 6 as a function of the reaction coordinate, ρ . Interestingly, the edge chain shows a stair-step type of free energy profile. The middle chain, however, exhibits a smoother free energy profile. The free energy values for the edge and middle chains can be separated into a per chitobiose unit by dividing the final free energy value by 5 (for pulling out 5 dimer units). We note that implicit in this analysis is the assumption that the decrystallization process is noncooperative. Thus, the free energy to decrystallize an edge chain in α -chitin is 5.6 ± 0.22 kcal/mol per chitobiose and for a middle chain we obtain 8.0 ± 0.60 kcal/mol per chitobiose. The work to decrystallize edge chains in α -chitin interestingly is equal (within error) to that of cellulose I β . The α -chitin middle chain, however exhibits ~ 1.5 kcal/mol per chitobiose free energy penalty higher than in cellulose I β .

We also examined the molecular reasons for the stair-step behavior in the edge chain decrystallization free energy profile relative to the middle chain, which yields a smoother free energy profile. We observed in both the equilibration and the umbrella sampling simulations for the edge chain that there were fewer bifurcated hydrogen bonds on the side of the crystal where the chain is more exposed to water. This is due to hydrogen bonding of the GlcNAc side chains with water, which weakens the hydrogen bond network on the solvent exposed face of the edge chain. However, the bifurcated hydrogen bonds on the side of the

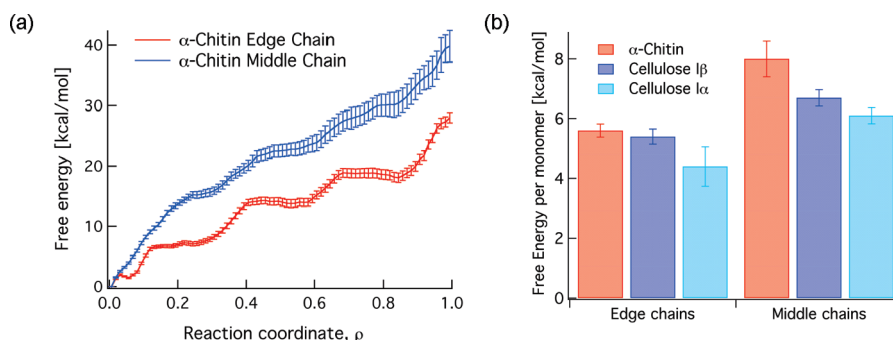


Figure 6. (a) Free energy profile as a function of the reaction coordinate, r , of decrystallization of chitin chains from an edge chain and a middle chain. (b) Chitin decrystallization free energy per chitobiose compared to native cellulose I β and I α per cellobiose. The cellulose results are from ref 27. Errors are standard errors of the mean.

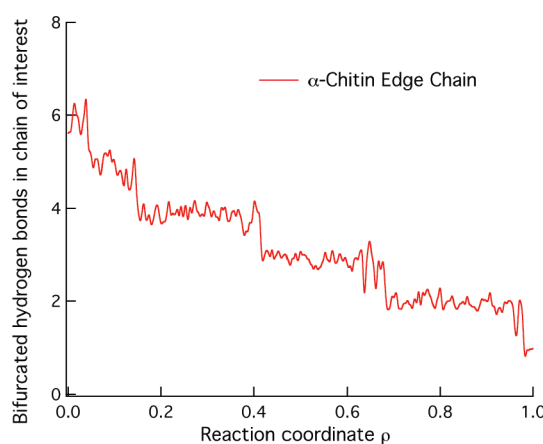


Figure 7. Bifurcated hydrogen bonds as a function of the reaction coordinate, r , for the α -chitin edge chain.

edge chain that are interior to the crystal are quite stable, and in the umbrella sampling simulations the disruption of these hydrogen bonds along ρ corresponds to the new plateaus reached in the free energy profile. This is illustrated in Figure 7, which shows the number of the bifurcated hydrogen bonds for the edge chain. The middle chain, which has more stable bifurcated hydrogen bonds on each side (because the hydrogen bonds are not exposed to solvent), exhibits a continuous decrease in hydrogen bonds and thus a smoother free energy landscape.

As with cellulose, these results imply that chitin chains on the edges of crystals are substantially easier (by 3 kcal/mol per chitobiose) to decrystallize for an enzyme than middle chains on the surface. Thus for processive chitinases, it is likely that corner chains are digested preferentially. However, like in cellulose, it is difficult to assign the shapes of microfibrils that are synthesized by organisms in Nature, but the microfibril shape is key to a complete understanding of chitin deconstruction. This is because the shape of the microfibril and the population of chains on the surface will have a significant effect on the macroscopically observed conversion rate for chitinases. Here we have addressed the question of the thermodynamic work at the nanoscale, and with experimentally determined shapes of chitin polymer crystals these data could be used directly to build kinetic, morphology-based models of deconstruction of chitin by a cocktail of chitinase enzymes, as has been done for cellulose by several groups.^{53–55}

From the standpoint of the stability and insoluble nature of crystalline chitin, here we have calculated the amount of work to

remove monomers from the surface. Our results indicate that a middle chain is stabilized by a significant thermodynamic penalty of 8 kcal/mol per chitobiose unit. In Nature, chitin chains are typically on the order of 10^2 to 10^3 units long. Thus the quantities calculated here shed light on the incredible stability of chitin and the molecular level reasons that it is such a hardy structural and defense material for organisms in the biosphere.

From a computational standpoint, the approach described here can be readily deployed to understand the structure, dynamics, and decrystallization thermodynamics of other crystals of chitin, such as the hydrate and anhydrous forms of β -chitin¹⁴ as well as other polymer crystals where the unit cell structures are known (beyond carbohydrate polymers as well). We will conduct this study for β -chitin in future work. Given the wealth of new structural data on chitinase enzymes^{15–17,20} and other biomolecules that work on chitin,^{56–58} this study indicates the morphological features of α -chitin for constructing and simulating chitin-active enzymes on insoluble chitin. These types of simulations will enable elucidation of the structures of catalytically active complexes of chitinases on chitin crystals, which is typically inaccessible in experiments. In addition, this work is related directly to the recent set of studies from Sorlie et al. on understanding ligand-binding free energies in chitinase enzymes.^{22–26} The experimentally determined values of ligand-binding free energy in these thermodynamic studies are experimental measures of the compensating binding free energy that enzymes must exhibit to decrystallize individual chitin chains, as calculated in this study.

CONCLUSIONS

Here we have conducted MD simulations of α -chitin with the aim to understand the molecular origins for its recalcitrance. With the newly developed C35 CHARMM force field for carbohydrates, we find excellent agreement with the recently refined crystal structure.¹¹ Using large-scale free energy simulations, we have calculated the intrinsic work to decrystallize edge and middle chains in α -chitin. The work calculated here must be overcome by chitinase enzymes via their ligand-binding free energy of chitin chains in their tunnels or clefts. Compared to natural cellulose I β , α -chitin exhibits nearly comparable decrystallization work for edge chains and higher work for middle chains. However, unlike cellulose I β and I α , the work that a chitinase enzyme must conduct to decrystallize chains from α -chitin is dominated by a single bifurcated hydrogen bond to adjacent layers of chains. This work will enable further studies of

chitin and with new crystal structures of chitin-active enzymes, it will enable computational approaches to resolve catalytically active complexes and study reaction mechanisms on insoluble substrates.

■ ASSOCIATED CONTENT

Supporting Information. Additional figures and table. This material is available free of charge via the Internet at <http://pubs.acs.org>.

■ AUTHOR INFORMATION

Corresponding Author

*E-mail: gregg.beckham@nrel.gov.

■ ACKNOWLEDGMENT

Computer time was provided by the TACC Ranger cluster under the National Science Foundation Teragrid Grant MCB090159 and by the NREL Computational Sciences Center supported by the DOE Office of EERE under Contract Number DE-AC36-08GO28308. We acknowledge use of Alan Grossfield's WHAM code. All figures were made with VMD 1.8.7.⁵⁹ We thank James Matthews, Yannick Bomble, Michael Himmel, and Baron Peters for helpful discussions.

■ REFERENCES

- (1) Latge, J. P. The cell wall: a carbohydrate armour for the fungal cell. *Mol. Microbiol.* **2007**, *66*, 279–290.
- (2) Lenardon, M. D.; Munro, C. A.; Gow, N. A. R. Chitin synthesis and fungal pathogenesis. *Curr. Opin. Microbiol.* **2010**, *13*, 416–423.
- (3) Rinaudo, M. Chitin and chitosan: Properties and applications. *Prog. Polym. Sci.* **2006**, *31*, 603–632.
- (4) Crini, G. Recent developments in polysaccharide-based materials used as adsorbents in wastewater treatment. *Prog. Polym. Sci.* **2005**, *30*, 38–70.
- (5) Neeraja, C.; Anil, K.; Purushotham, P.; Suma, K.; Sarma, P.; Moerschbacher, B. M.; Podile, A. R. Biotechnological approaches to develop bacterial chitinases as a bioshield against fungal diseases of plants. *Crit. Rev. Biotechnol.* **2010**, *30*, 231–241.
- (6) Pillai, C. K. S.; Paul, W.; Sharma, C. P. Chitin and chitosan polymers: Chemistry, solubility and fiber formation. *Prog. Polym. Sci.* **2009**, *34*, 641–678.
- (7) Tharanathan, R. N.; Kittur, F. S. Chitin - The undisputed biomolecule of great potential. *Crit. Rev. Food Sci. Nutr.* **2003**, *43*, 61–87.
- (8) Zhou, Y. F.; Haynes, R. J. Sorption of Heavy Metals by Inorganic and Organic Components of Solid Wastes: Significance to Use of Wastes as Low-Cost Adsorbents and Immobilizing Agents. *Crit. Rev. Environ. Sci. Technol.* **2010**, *40*, 909–977.
- (9) Kumar, M. A review of chitin and chitosan applications. *React. Funct. Polym.* **2000**, *46*, 1–27.
- (10) Langan, P.; Nishiyama, Y.; Chanzy, H. X-ray structure of mercerized cellulose II at 1 Å resolution. *Biomacromolecules* **2001**, *2*, 410–416.
- (11) Sikorski, P.; Hori, R.; Wada, M. Revisit of alpha-Chitin Crystal Structure Using High Resolution X-ray Diffraction Data. *Biomacromolecules* **2009**, *10*, 1100–1105.
- (12) Minke, R.; Blackwell, J. Structure of alpha chitin. *J. Mol. Biol.* **1978**, *120*, 167–181.
- (13) Gardner, K. H.; Blackwell, J. Refinement of structure of β-chitin. *Biopolymers* **1975**, *14*, 1581–1595.
- (14) Kobayashi, K.; Kimura, S.; Togawa, E.; Wada, M. Crystal transition between hydrate and anhydrous beta-chitin monitored by synchrotron X-ray fiber diffraction. *Carbohydr. Polym.* **2010**, *79*, 882–889.
- (15) Eijsink, V. G. H.; Vaaje-Kolstad, G.; Varum, K. M.; Horn, S. J. Towards new enzymes for biofuels: lessons from chitinase research. *Trends in Biotech.* **2008**, *26*, 228–235.
- (16) van Aalten, D. M. F.; Komander, D.; Synstad, B.; Gaseidnes, S.; Peter, M. G.; Eijsink, V. G. H. Structural insights into the catalytic mechanism of a Family 18 exo-chitinase. *Proc. Natl. Acad. Sci. U.S.A.* **2001**, *98*, 8979–8984.
- (17) van Aalten, D. M. F.; Synstad, B.; Brurberg, M. B.; Hough, E.; Riise, B. W.; Eijsink, V. G. H.; Wierenga, R. K. Structure of a two-domain chitotriosidase from *Serratia marcescens* at 1.9 Å resolution. *Proc. Natl. Acad. Sci. U.S.A.* **2000**, *97*, 5842–5847.
- (18) Horn, S. J.; Sikorski, P.; Cederkvist, J. B.; Vaaje-Kolstad, G.; Sorlie, M.; Synstad, B.; Vriend, G.; Varum, K. M.; Eijsink, V. G. H. Costs and benefits of processivity in enzymatic degradation of recalcitrant polysaccharides. *Proc. Natl. Acad. Sci. U.S.A.* **2006**, *103*, 18089–18094.
- (19) Zakariassen, H.; Aam, B. B.; Horn, S. J.; Varum, K. M.; Sorlie, M.; Eijsink, V. G. H. Aromatic residues in the catalytic center of chitinase A from *Serratia marcescens* affect processivity, enzyme activity, and biomass converting efficiency. *J. Biol. Chem.* **2009**, *284*, 10610–10617.
- (20) Sikorski, P.; Sorbotten, A.; Horn, S. J.; Eijsink, V. G. H.; Varum, K. M. *Serratia marcescens* chitinases with tunnel-shaped substrate-binding grooves show endo activity and different degrees of processivity during enzymatic hydrolysis of chitosan. *Biochemistry* **2006**, *45*, 9566–9574.
- (21) Horn, S. J.; Sorbotten, A.; Synstad, B.; Sikorski, P.; Sorlie, M.; Varum, K. M.; Eijsink, V. G. H. Endo/exo mechanism and processivity of Family 18 chitinases produced by *Serratia marcescens*. *FEBS J.* **2006**, *273*, 491–503.
- (22) Baban, J.; Fjeld, S.; Sakuda, S.; Eijsink, V. G. H.; Sorlie, M. The Roles of Three *Serratia marcescens* chitinases in Chitin Conversion Are Reflected in Different Thermodynamic Signatures of Allosamidin Binding. *J. Phys. Chem. B* **2010**, *114*, 6144–6149.
- (23) Cederkvist, F. H.; Saua, S. F.; Karlsen, V.; Sakuda, S.; Eijsink, V. G. H.; Sorlie, M. Thermodynamic analysis of allosamidin binding to a Family 18 chitinase. *Biochemistry* **2007**, *46*, 12347–12354.
- (24) Norberg, A. L.; Eijsink, V. G. H.; Sorlie, M. Dissecting factors that contribute to ligand-binding energetics for Family 18 chitinases. *Thermochim. Acta* **2010**, *511*, 189–193.
- (25) Norberg, A. L.; Karlsen, V.; Hoell, I. A.; Bakke, I.; Eijsink, V. G. H.; Sorlie, M. Determination of substrate binding energies in individual subsites of a Family 18 chitinase. *FEBS Lett.* **2010**, *584*, 4581–4585.
- (26) Zakariassen, H.; Eijsink, V. G. H.; Sorlie, M. Signatures of activation parameters reveal substrate-dependent rate determining steps in polysaccharide turnover by a Family 18 chitinase. *Carbohydr. Polym.* **2010**, *81*, 14–20.
- (27) Beckham, G. T.; Matthews, J. F.; Peters, B.; Bomble, Y. J.; Himmel, M. E.; Crowley, M. F. Molecular Level Origins of Biomass Recalcitrance: Decrystallization of Four Common Cellulose Polymorphs. *J. Phys. Chem. B* **2011** 10.1021/jp1106394.
- (28) Beckham, G. T.; Bomble, Y. J.; Bayer, E. A.; Himmel, M. E.; Crowley, M. F. Applications of computational science for understanding enzymatic deconstruction of cellulose. *Curr. Opin. Biotechnol.* **2011** 10.1016/j.copbio.2010.11.005.
- (29) Chundawat, S. P. S.; Beckham, G. T.; Himmel, M. E.; Dale, B. E.; Deconstruction of lignocellulosic biomass to fuels and chemicals. *Annu. Rev. Chem. Biomol. Eng.* **2011**, DOI: 10.1146/annurev-chem-bioeng-061010-114205.
- (30) Bellesia, G.; Asztalos, A.; Shen, T. Y.; Langan, P.; Redondo, A.; Gnanakaran, S. In silico studies of crystalline cellulose and its degradation by enzymes. *Acta Crystallogr., Sect. D* **66**:1184–1188.
- (31) Brooks, B. R.; Brooks, C. L., III; Mackerell, A. D., Jr.; Nilsson, L.; Petrella, R. J.; Roux, B.; Won, Y.; Archontis, G.; Bartels, C.; Boresch, S.; Cafisch, A.; Caves, L.; Cui, Q.; Dinner, A. R.; Feig, M.; Fischer, S.; Gao, J.; Hodoscek, M.; Im, W.; Kuczera, K.; Lazaridis, T.; Ma, J.;

- Ovchinnikov, V.; Paci, E.; Pastor, R. W.; Post, C. B.; Pu, J. Z.; Schaefer, M.; Tidor, B.; Venable, R. M.; Woodcock, H. L.; Wu, X.; Yang, W.; York, D. M.; Karplus, M. CHARMM: the biomolecular simulation program. *J. Comput. Chem.* **2009**, *30*, 1545–1614.
- (32) Nosé, S.; Klein, M. L. Constant pressure molecular dynamics for molecular systems. *Mol. Phys.* **1983**, *50*, 1055–1076.
- (33) Hoover, W. G. Canonical dynamics - equilibrium phase-space distributions. *Phys. Rev. A* **1985**, *31*, 1695–1697.
- (34) Guvench, O.; Greene, S. N.; Kamath, G.; Brady, J. W.; Venable, R. M.; Pastor, R. W.; Mackerell, A. D. Additive Empirical Force Field for Hexopyranose Monosaccharides. *J. Comput. Chem.* **2008**, *29*, 2543–2564.
- (35) Guvench, O.; Hatcher, E.; Venable, R. M.; Pastor, R. W.; MacKerell, A. D. CHARMM additive all-atom force field for glycosidic linkages between hexopyranoses. *J. Chem. Theor. Comp.* **2009**, *5*, 2353–2370.
- (36) Jorgensen, W. L.; Chandrasekhar, J.; Madura, J. D. Comparison of simple potential functions for simulating liquid water. *J. Chem. Phys.* **1983**, *79*, 926–935.
- (37) Ryckaert, J.; Ciccotti, G.; Berendsen, H. J. *Comput. Phys.* **1977**, *23*.
- (38) Essmann, U.; Perera, L.; Berkowitz, M. L.; Darden, T.; Lee, H.; Pedersen, L. G. A smooth particle mesh Ewald method. *J. Chem. Phys.* **1995**, *103*, 8857.
- (39) Gross, A. S.; Chu, J. W. On the Molecular Origins of Biomass Recalcitrance: The Interaction Network and Solvation Structures of Cellulose Microfibrils. *J. Phys. Chem. B* **2010**, *114*, 13333–13341.
- (40) Matthews, J. F.; Skopec, C. E.; Mason, P. E.; Zuccato, P.; Torget, R. W.; Sugiyama, J.; Himmel, M. E.; Brady, J. W. Computer simulations of microcrystalline cellulose I β . *Carb. Res.* **2006**, *341*, 138–152.
- (41) Bergenstråhl, M.; Berglund, L. A.; Mazeau, K. Thermal Response in Crystalline I Beta Cellulose: A Molecular Dynamics Study. *J. Phys. Chem. B* **2007**, *111*, 9138–9145.
- (42) Yui, T.; Hayashi, S. Molecular dynamics simulations of solvated crystal models of cellulose I-alpha and III. *Biomacromolecules* **2007**, *8*, 817–824.
- (43) Lehtiö, J.; Sugiyama, J.; Gustavsson, M.; Fransson, L.; Linder, M.; Teeri, T. T. The binding specificity and affinity determinants of Family 1 and Family 3 cellulose binding modules. *Proc. Natl. Acad. Sci. U.S.A.* **2003**, *100*, 484–489.
- (44) Beckham, G. T.; Matthews, J. F.; Bomble, Y. J.; Bu, L.; Adney, W. S.; Himmel, M. E.; Nimlos, M. R.; Crowley, M. F. Identification of Amino Acids Responsible for Processivity in a Family 1 Carbohydrate-Binding Module from a Fungal Cellulase. *J. Phys. Chem. B* **2010**, *114*, 1447–1453.
- (45) Bu, L.; Beckham, G. T.; Crowley, M. F.; Chang, C. H.; Matthews, J. F.; Bomble, Y. J.; Adney, W. S.; Himmel, M. E.; Nimlos, M. R. The Energy Landscape for the Interaction of the Family 1 Carbohydrate-Binding Module and the Cellulose Surface Is Altered by Hydrolyzed Glycosidic Linkages. *J. Phys. Chem. B* **2009**, *113*, 10994–11002.
- (46) Torrie, G. M.; Valleau, J. P. Non-physical sampling distributions in Monte-Carlo free-energy estimation - umbrella sampling. *J. Comput. Phys.* **1977**, *23*, 187–199.
- (47) Kottalam, J.; Case, D. A. Dynamics of Ligand Escape from the Heme Pocket of Myoglobin. *J. Am. Chem. Soc.* **1988**, *110*, 7690–7697.
- (48) Sheinerman, F. B.; Brooks, C. L. Calculations on folding of segment B1 of streptococcal protein G. *J. Mol. Biol.* **1998**, *278*, 439–456.
- (49) Kumar, S.; Rosenberg, J. M.; Bouzida, D.; Swendsen, R. H.; Kollman, P. A. The weighted histogram analysis method for free-energy calculations on biomolecules. I. The method. *J. Comput. Chem.* **1992**, *13*, 1011–1021.
- (50) Beckham, G. T.; Peters, B.; Starbuck, C.; Variankaval, N.; Trout, B. L. Surface-Mediated Nucleation in the Solid-State Polymorph Transformation of Terephthalic Acid. *J. Am. Chem. Soc.* **2007**, *129*, 4714–4723.
- (51) Day, G. M.; Motherwell, W. D. S.; Ammon, H. L.; Boerriger, S. X. M.; Della Valle, R. G.; Venuti, E.; Dzyabchenko, A.; Dunitz, J. D.; Schweizer, B.; van Eijck, B. P.; Erk, P.; Facelli, J. C.; Bazterra, V. E.; Ferraro, M. B.; Hofmann, D. W. M.; Leusen, F. J. J.; Liang, C.; Pantelides, C. C.; Karamertzaris, P. G.; Price, S. L.; Lewis, T. C.; Nowell, H.; Torrisi, A.; Scheraga, H. A.; Arnautova, Y. A.; Schmidt, M. U.; Verwer, P. A third blind test of crystal structure prediction. *Acta Crystallogr., Sect. B* **2005**, *61*, 511–527.
- (52) Woodley, S. M.; Catlow, R. Crystal structure prediction from first principles. *Nat. Mater.* **2008**, *7*, 937–946.
- (53) Bansal, P.; Hall, M.; Realff, M. J.; Lee, J. H.; Bommarius, A. S. Modeling cellulase kinetics on lignocellulosic substrates. *Biotechnol. Adv.* **2009**, *27*, 833–848.
- (54) Zhou, W.; Hao, Z. Q.; Xu, Y.; Schuttler, H. B. Cellulose Hydrolysis in Evolving Substrate Morphologies II: Numerical Results and Analysis. *Biotechnol. Bioeng.* **2009**, *104*, 275–289.
- (55) Zhou, W.; Schuttler, H. B.; Hao, Z. Q.; Xu, Y. Cellulose Hydrolysis in Evolving Substrate Morphologies I: A General Modeling Formalism. *Biotechnol. Bioeng.* **2009**, *104*, 261–274.
- (56) Harris, P. V.; Welner, D.; McFarland, K. C.; Re, E.; Poulsen, J. C. N.; Brown, K.; Salbo, R.; Ding, H. S.; Vlasenko, E.; Merino, S.; Xu, F.; Cherry, J.; Larsen, S.; Lo Leggio, L. Stimulation of Lignocellulosic Biomass Hydrolysis by Proteins of Glycoside Hydrolase Family 61: Structure and Function of a Large, Enigmatic Family. *Biochemistry* **2010**, *49*, 3305–3316.
- (57) Vaaje-Kolstad, G.; Houston, D. R.; Riemen, A. H. K.; Eijsink, V. G. H.; van Aalten, D. M. F. Crystal structure and binding properties of the *Serratia marcescens* chitin-binding protein CBP21. *J. Biol. Chem.* **2005**, *280*, 11313–11319.
- (58) Vaaje-Kolstad, G.; Westereng, B.; Horn, S. J.; Liu, Z. L.; Zhai, H.; Sorlie, M.; Eijsink, V. G. H. An Oxidative Enzyme Boosting the Enzymatic Conversion of Recalcitrant Polysaccharides. *Science* **2010**, *330*, 219–222.
- (59) Humphrey, W.; Dalke, A.; Schulter, K. VMD: Visual molecular dynamics. *J. Mol. Graph.* **1996**, *14*, 33–&.